RSC Advances

PAPER

View Article Online
View Journal | View Issue

Cite this: *RSC Adv.*, 2025, **15**, 27260

Integration of RNN and CatBoost models in a tea-waste biochar filtration system for toxic organic pollutant removal efficiency prediction†

Stuti Jha,[a] Rama Gaur, *[a] Syed Shahabuddin,*[a] Vinay Vakharia [b] and Mohammed E. Ali Mohsin*[c]

Water pollution is a dreadful global crisis undermining the environment and economy. In order to combat this issue, several methods and techniques are adopted for treating the polluted water. Adsorption by biowastes is one of the most economically viable, simple, and effective methods for wastewater treatment. In spite of numerous reports in the literature showing the removal of various pollutants, there is still room for investigation in the field of simultaneous adsorption of varied categories of pollutants. The present study focuses on the simultaneous removal of organic water contaminants like dyes, agrochemicals, and aromatic compounds from wastewater using biochar prepared from tea waste as adsorbent. A detailed investigation on the effect of contact time, pH, dosage, and temperature on the adsorption performance of adsorbent has been carried out. At optimized reaction condition of 5 mg ml^{-1} of adsorbent dosage at pH 2 for 60 min, 82.66% overall removal was obtained for 40 ppm of pollutant (malachite green, congo red, chlorpyrifos, and 4-nitroaniline) mixture. Further, the percentage removal was predicted using two machine learning (ML) models: CatBoost and Recurrent Neural Network (RNN), with and without Bayesian optimization. The prediction capability of these models was evaluated using three performance metrics: coefficient of determination (R^2), Mean Absolute Error (MAE), and Root Mean Square Error (RMSE). Based on the evaluation, RNN was found to be the most effective model for % removal prediction based on higher R^2 value of 0.960. Moreover, the fabrication of a portable column filtration device for the removal of coexisting harmful organic pollutants has been demonstrated. The results confirm that tea waste (TW)-derived biochar, coupled with advanced machine learning models, is a promising solution for real-time wastewater treatment.

Received 12th February 2025
Accepted 19th July 2025

DOI: 10.1039/d5ra01021g

rsc.li/rsc-advances

1. Introduction

Water is a vital element for life and a key to survival. Approximately two thirds of the world's population experience water scarcity problems or lack access to clean/pure water. Thus, it is a global priority to preserve water quantity and quality. Besides overpopulation, climate change, exploitation of various water resources, *etc.* water pollution is also one of the chief causes of water being unfit for usage and shortage of freshwater availability.[1,2] Water pollution has risen at an alarming rate due to anthropogenic activities like industrialization, enlargement of urban areas, metropolitan expansion, and mining practises over the years. Effluents and overspills from different industries such food, textiles, leather, pharmaceuticals, tannery, and oil refining are the leading sources of water pollution.[3] Wastewater constitutes of persistent organic and inorganic water contaminants like dyes, agrochemicals, aromatic compounds, heavy metals, oil-spills, *etc.*[4,5] These toxic chemicals inflict havoc on human well-being and wildlife eventually leading to an imbalance in the ecosystem. To battle this peril of water pollution, extensive research has been carried out in the area of wastewater treatment. A great deal of efforts has been invested towards the development of effective techniques and materials for the treatment of wastewater. Various cost-effective techniques like photocatalysis, reverse osmosis, chemical precipitation, ion-exchange, *etc.* are employed for the treatment of wastewater.[6] However, there are certain disadvantages like fouling of membrane, complex operational conditions and set-up, limited efficiency, generation of sludge, *etc.* associated with these methods. Adsorption is one such cost-effective, simple, widely adapted, and efficient method for removal of noxious pollutants from wastewater.[7,8] Some of the most common adsorbents include zeolites, carbon-based materials, nanomaterials, bio-wastes, activated carbon, *etc.*[9–11] A large

[a]*Department of Chemistry, School of Energy Technology, Pandit Deendayal Energy University, Knowledge Corridor, Raysan, Gandhinagar, Gujarat 382426, India. E-mail: rama.gaur@sot.pdpu.ac.in; syed.shahabuddin@sot.pdpu.ac.in*

[b]*Department of Mechanical Engineering, School of Technology, Pandit Deendayal Energy University, Knowledge Corridor, Raysan, Gandhinagar, Gujarat 382426, India*

[c]*Department of Chemical Engineering, College of Engineering, King Faisal University, Al Ahsa 31982, Saudi Arabia. E-mail: maa.ali@kfu.edu.sa*

† Electronic supplementary information (ESI) available. See DOI: https://doi.org/10.1039/d5ra01021g

number of reports are available in the literature focusing on adsorption of a single pollutant and a few focusing on simultaneous removal (binary or multicomponent system) of pollutants of same category (Table S1†).[12–23] As deduced from the literature search, there is lack of reports on:

(1) Simultaneous removal of pollutants from a diverse range of pollutants.

(2) Large scale application of adsorbent.

(3) An adsorption study on real-time industrial effluent.

There is always an expected co-existence of multiple pollutants with different structure, charges, chemical nature *etc.* in wastewater.[24] Therefore, for an adsorbent to be an ideal candidate for wastewater treatment, it needs to be effective in not just individual removal but simultaneous removal of pollutants as well. Apart from that as the industry scale adsorption employs column filtration considering the high volume of wastewater, the practicality and efficiency of the adsorbent should not be limited to laboratory scale only. Fabrication and designing of a portable column filtration system is a simple, convenient, and effective way for large-scale wastewater treatment.[25] Thus, development and detailed investigation of adsorbents offering the merits of being low-cost, multi-functional, and effective for both lab as well as real-time large-scale analysis is a pressing priority in the area of water treatment and environmental remediation.[26] In the present study, biochar which is a carbon-rich, green, and effective adsorbent prepared from pyrolysis of biowastes has been utilized for abatement of organic pollutants. Apart from carbon, biochar's composition consists of significant amount of oxygen, hydrogen, and nitrogen. The specific properties of biochar include long-term stability, hydrophobicity, large surface area, chemical composition, high porosity, *etc.* which is hypothesized to promote interaction with pollutants and make them a suitable candidate for adsorption.[27,28] The pyrolysis temperatures for preparation of biochar *i.e.* 300 °C, 500 °C, 700 °C were chosen with an aim to have biochar prepared at mild, moderate, and extreme pyrolysis temperature. Also, the properties of biochar are deeply influenced by the pyrolysis temperature so selecting the temperature from a broad zone enables obtaining adsorbents with distinct nature. For example, at 300 °C, biochar generally retains a high concentration of oxygen-containing functional groups (*e.g.*, –OH, –COOH), which enhance adsorption through hydrogen bonding and electrostatic interactions, particularly beneficial for binding polar pollutants. At 500 °C, more conversion to carbon can be observed and aromaticity is introduced in the biochar. At high temperature of 700 °C, ash content increases in the biochar and agglomeration of particles can also expected.

Machine learning in adsorption studies refers to the use of data-driven algorithms to predict adsorption efficiency based on various input parameters such as adsorbent properties, pollutant concentration, pH, and contact time. By analyzing experimental data (*e.g.*, pollutant type, concentration, pH, contact time, and removal %), machine learning can identify key influencing factors affecting the percentage of adsorption and its prediction. In this study, machine learning was applied to predict the removal efficiency of toxic pollutants using biochar, enabling accurate estimation based on input variables such as adsorbent dosage, contact time, and initial pollutant concentration. This approach enhances the understanding and optimization of biochar-based adsorption. Optimization techniques ensure the selection of hyperparameter of ML models which significantly enhances the predictive performance of models. Furthermore, ML-driven comprehension of biochar properties and pollutant behaviour aids in the development of more effective and sustainable filtration techniques. Zhang *et al.* examines the utility of ML to predict the biochar yield and properties from biomass residue.[29] Authors emphasizes how anaerobic digestion processes enhanced by biochar may be optimized using machine learning to recover bioenergy. Chang and Lee predicts the adsorption characteristics of biochar-activated carbon generated from waste wood using artificial neural network to optimize production efficiency and cost.[30] The results highlight ML potential to enhance adsorption performance and process optimization. In another study, Zhang *et al.* highlights the potential use of ML to optimize the synthesis and adsorption capacities of biochar for the elimination of contaminants.[31] Study systematically covers advancements in predicting biochar yield, physicochemical properties, adsorption efficiency, and optimal conditions while providing general guidelines for whole-process optimization.

Prior studies on pollutant removal efficiency predicts mostly used traditional experimental methods and simpler statistical models, which often had scalability and accuracy issues. However, in this study, authors anticipate the percentage of elimination by using the advanced capabilities of RNN and CatBoost models. While RNNs succeed at capturing temporal and sequential correlations in adsorption processes, CatBoost excels at handling categorical information and complex interactions. In the absence of Bayesian optimization, these models provide baseline projections using default configurations, offering insight into the underlying trends in pollutant removal. Bayesian optimization is used to systematically modify hyperparameters in order to increase accuracy, decrease errors, and provide dependable outcomes. This dual approach allows for a comparative evaluation of model performance and demonstrates how machine learning may be used to improve biochar-based filtration systems for simultaneous pollution removal. With these models, authors aim to set a benchmark for predictive analytics in wastewater treatment processes.

The significant contribution of present study is as follows:

(a) The work addresses the challenging issue of multi-pollutant adsorption in synthetic wastewater by concentrating on the simultaneous removal of agrochemicals, dyes, and aromatic compounds. Based on the widespread availability of tea waste in the Indian context, their unique physical and chemical properties, and large amount of tea waste (approximately 25 million kilogram) generated in India in a year due to its high consumption, the biowaste (tea waste) has been chosen for the preparation of biochar (pyrolysis at 300 °C, 500 °C, and 700 °C, for 3 hours at 5 °C min^{-1} of heating rate).[32]

(b) It also focuses on the effect of various parameters like contact time, dosage, pH, and temperature on the adsorption process.

(c) The study offers a portable device for real-time wastewater treatment that incorporates machine learning insights and offers

Table 1 Structure, charge and toxic effect of the pollutants studied in the present report

Pollutant	Structure	Charge	Toxic effect	Ref
Malachite green (MG)	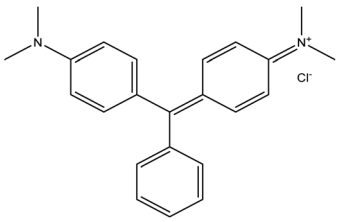	+ve	Respiratory toxicity, carcinogenic, chromosomal fractures	33
Congo red (CR)	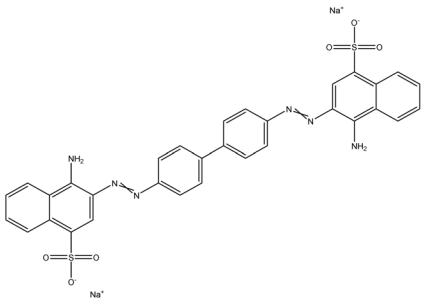	−ve	Carcinogenic, mutagenic, causes infertility, irritation to skin	34
4-Nitro aniline (4-NA)	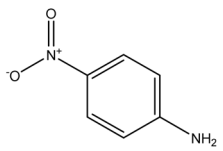	−ve	Dizziness, fatigue, methemoglobinemia, anemia	35
Chlorpyrifos (CPY)	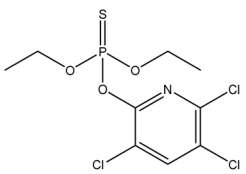	−ve	Headaches, blurred vision, muscle tremors, endocrine disruption	36

a scalable, practical solution for large-scale applications, all while using a comprehensive adsorption mechanism for each pollutant.

(d) This study utilizes RNN and CatBoost to properly predict % removal efficiency, utilizing their capabilities in handling sequential data and complicated interactions, in contrast to prior studies that relied on conventional experimental approaches and simple statistical models.

(e) Using Bayesian optimization to fine-tune RNN and CatBoost hyperparameters sets guidelines for ML applications in wastewater treatment, ensuring improved prediction accuracy, fewer errors, and reliable outcomes. The nature of these pollutants along with their structure, charge, and toxic impacts is as listed in Table 1.[33–36]

2. Material and method

The detailed discussion on chemicals and materials used during the present study has been done in Section 2.1 and 2.2.

2.1. Materials

The TW required for the preparation of biochar was collected from the canteen of Pandit Deendayal Energy University, Gandhinagar, India. Other chemicals: acetone (Finar, AR grade, purity: 99%), $NaNO_3$ (Merck, ACS grade, purity: 99%), HCl (Finar, AR grade, purity: 37%), NaOH (Merck, ACS grade, purity: 97%), malachite green (MG) (Finar, extrapure, purity 90%), congo red (CR) (SRL chemical, ACS grade, purity: 75%), 4-nitroaniline (4-NA) (Sigma-Aldrich, purity: 99%), and chlorpyrifos (CPY) (commercial, SUPER-D, $\rho = 1.4$ g cm^{-3}) were used as received. In this study, millipore water was used for preparing all the solutions.

2.2. Pre-treatment of tea waste

The collected TW was thoroughly rinsed washed with distilled water and shade-dried. The dried TW was crushed in a mixer grinder to convert it into powdered form. The powder obtained was sieved with a sieve (mesh size <75 μm) to obtain uniform-sized particles of TW (75 μm). TW powder was stored in air-tight vials to avoid atmospheric moisture adsorption.

2.3. Preparation of biochar from tea waste

Pyrolysis method was used for the preparation of biochar. The sieved TW powder was weighed and kept in a crucible inside the muffle furnace (Thermo fisher). The biochar was prepared at three different pyrolysis temperatures (300 °C, 500 °C, and 700 °C) for 3 hours with the heating rate of 5 °C min^{-1} and will be here forth referred to as TW3, TW5, and TW7, respectively.

3. Characterization

All the samples in the current study were analyzed for their functional groups, crystallinity, morphology, surface area, and surface charge. The Fourier-transform infrared (FTIR) spectra of the samples were recorded using FTIR spectrometer PerkinElmer, spectrum 2 model in ATR mode (scan range of 400–4000 cm^{-1}) for estimating the functional groups present. The X-ray diffraction spectra (XRD) was recorded using PANalytical X'Pert Pro diffractometer at 40 kV using filtered Cu Kα radiation ($\lambda = 1.53$ Å) with a goniometer speed in 5 to 50°, 2θ range (step size = 1° per minute). The morphology of the samples was studied using field emission-scanning electron microscopy (FE-SEM) images of the samples taken in Zeiss ultra 55 model at acceleration voltage of 5.00 kV. For FE-SEM analysis the samples were sprinkled on clean aluminum stub over conducting carbon tape. A thin gold layer was coated on the stubs using LEICA EM ACE200 to make them conductive. The surface area was calculated by Brunauer–Emmett–Teller (BET) analysis in Altamira BET analyzer at a degassing temperature of 200 °C for 2 hours. The charge on the adsorbent surface was analyzed using point of zero charge (PZC) method using salt addition method.[37] LABINDIA 3000+ Ultraviolet-visible (UV-vis) Spectrophotometer was used to monitor the concentration of the analyte solutions during the entire adsorption study.

4. Adsorption study

The model pollutants (CPY, 4-NA, MG, and CR) were removed using TW, TW3, TW5, and TW7. The primary investigation was carried out by performing individual removal studies. Based on the results, the best adsorbent was selected for an in-depth adsorption analysis for simultaneous removal. The adsorption studies were conducted for individual removal and simultaneous removal of the chosen pollutants from synthetic wastewater. All the adsorption studies were performed at room temperature. For individual and simultaneous removal 10 ppm solution of individual analyte and a mixture (40 ppm) of all the analytes, respectively were prepared. The effective concentration of all the analyte was kept as 10 ppm in all the adsorption studies. In a typical adsorption study 10 mg of adsorbent was added to 10 ml of the analyte solution. The solution was then sonicated for 5 minutes. The solutions were then placed on a shaker for 60 min for continuous stirring (170 rpm). After completion of 60 min, the solutions were centrifuged for 5 min at 4000 rpm to allow settling down of the adsorbent. The supernatant of the solutions was analysed using UV-visible spectrophotometer to monitor the concentration of the analytes. The λ_{max} values for MG, CR, 4-NA, and CPY during the individual adsorption were considered as 617 nm, 499 nm, 381 nm, 298 nm, respectively while during the simultaneous adsorption were found to be 648 nm, 516 nm, 361 nm, and 298 nm, respectively. A shift in the λ_{max} values in the mixture as compared to individual can be due to the interactions between the pollutant molecules in the mixture.

The kinetics, dosage, pH studies, isothermal, and thermodynamic studies were carried out for the simultaneous removal using the best selected adsorbent from the primary adsorption studies. The kinetic studies were performed by monitoring the concentration of the analyte solution at a regular time interval of 10 minutes up to 60 minutes till the attainment of equilibrium. The obtained kinetic data were fitted into different kinetic models namely first order (FO), second order (SO), Pseudo first order (PSO), Pseudo second order (PSO), Elovich, and intra-particle diffusion model. The effect of dosage and pH on the adsorption efficiency of the adsorbent was studied by varying the adsorbent dosage (0.1 mg ml^{-1} to 5 mg ml^{-1}) and pH of the analyte solution (2, 4, 7, 10, and 12). The acidic and basic pH were adjusted using 0.1 M HCl and 0.1 M NaOH. The spent adsorbent was collected and regenerated by washing with acetone followed by drying overnight at 60 °C. The isothermal studies were performed by varying the concentration analyte from 5 to 40 ppm. The effect of temperature was studied at different temperatures of 278 K, 288 K, 298 K, 318 K, and 323 K.

The column adsorption study was performed by packing a glass column sized 15 mm × 300 mm. 0.5 g (1 cm height) of adsorbent was packed between two layers of cotton. The analyte solutions containing mixture of pollutants with 10 ppm concentration, was fed into the adsorbent packed column *via* continuous flow with a vacuum pump (flow rate = 0.2 ml min^{-1}). The filtrate obtained after passing 100 ml of analyte solution through the column was analysed using UV-visible spectroscopy. The removal/adsorption (%) and adsorption capacity at equilibrium are calculated using eqn (1) and (2), respectively.

$$\%\ \text{Adsorption} = \frac{C_i - C_e}{C_i} \times 100 \quad (1)$$

where, C_i represents concentration of analyte before adsorption, C_e indicates concentration of the analyte at equilibrium

$$Q_e = V(C_1 - C_2) \div M \quad (2)$$

Q_e refers to adsorption capacity at equilibrium (mmol g^{-1}); V represents volume of analyte solution taken (ml); M stands for quantity of adsorbent added (mg); C_1 and C_2 refer to the analyte concentration before and after adsorption respectively at the λ_{max} value (mg L^{-1}).

5. Machine learning

ML is a type of artificial intelligence techniques which allows computers to learn from data and make judgments or predictions without explicit programming. In order to address difficult issues across a variety of fields, the task of ML is to find patterns and correlations in data. From image identification and natural language processing to intricate predictive modelling, it has several uses in manufacturing industries, environmental sciences, *etc.*[38] Large datasets and nonlinear interactions are easily handled by machine learning approaches including ensemble methods, decision trees, and neural networks. Recent developments have made ML a significant tool for process optimization, result prediction, and revealing insights that conventional approaches often overlook.[39] As

shown by its use in industries like wastewater treatment, machine learning model has the potential to completely transform real-world problem-solving by improving accuracy, efficiency, and scalability. In the present study, authors incorporated and tuned RNN and Catboost to predict % removal efficiency. The brief description of models are as follows.

5.1. Recurrent neural network

RNNs are a type of ANN designed to process sequential data by remembering previous inputs *via* internal states. Applications requiring temporal or sequential dependency, such as language modelling and time-series forecasting, benefit greatly from its use. The mathematical formulation of RNN is as follows:[40]

(a) Hidden state: RNN primary memory mechanism is the hidden state (Z_t). It allows the network to comprehend temporal or sequential linkages by storing data from earlier time steps (z_{t-1}). It is formulated as:

$$Z_t = \varphi(W_h z_{t-1} + W_u U_t + b_z) \quad (3)$$

Here W_h and W_u represents the weight matrix for previous hidden state and weight matrix for the input at time t. φ represent activation function and b_z represent bias vector.

(b) Output calculation: the output at time step t, denoted as O_t, is computed as:

$$O_t = \psi(W_o Z_t + b_o) \quad (4)$$

where W_o represents weight matrix to map hidden state to output state. Ψ represent the output activation function.

(c) Loss function: the performance of RNN is evaluated using a loss function, such as MSE for regression tasks or cross-entropy loss for classification which is computed as:

$$\varepsilon = \frac{1}{N}\sum_{t=1}^{N} l\left(O_t, \hat{O}_t\right) \quad (5)$$

Here, ε represent total loss in sequence, l loss function, O_t and $\hat{O}_t$ represent true and predicted value at time t.

5.2. CatBoost

Catboost also known as categorical boosting is a kind of gradient boosting algorithm which is specifically designed to perform efficiently with categorical data. The algorithms utilized decision tree as a base learner and incorporates order encoding and target-based encoding to enhance accuracy, and reduce overfitting. Here loss function is minimized by iteratively adding weak learners. The mathematical formulation is as follows:

(a) Objective function:

The loss function which needs to be minimized is as follows:

$$\varepsilon = \frac{1}{N}\sum_{t=1}^{N} l\left(t_i, \hat{t}_i\right) \quad (6)$$

(b) Gradient boosting framework:

The CatBoost model added new decision trees at each iteration and the prediction at step k is represented as:

$$\hat{t}_i^{(k)} = \hat{t}_i^{(k-1)} + \alpha\mu_k(V_i) \quad (7)$$

Here, $\hat{t}_i^{(k-1)}$ represent prediction at previous iteration, α represent learning rate, and μ_k represent output of kth decision tree.

(c) Categorical feature encoding:

It is mathematically represented as

$$\text{Encoded}(c) = \frac{\sum_{j=1}^{i-1} 1\left[C_j = C\right]\cdot t_j}{\sum_{j=1}^{i-1} 1\left[C_j = C\right]\cdot \beta} \quad (8)$$

Here, $1[C_j = C]\cdot t_j$ represent a function whose value equal to 1 if sample j has same category as C. t_j represent target value for sample j. β represents smoothing parameter to prevent overfitting.

(d) Symmetric trees:

When CatBoost builds symmetric decision trees, every leaf splits on the same feature at the same depth. The gain function is maximized to define the tree structure as follows:

$$\text{Gain} = \sum \frac{G_l^2}{H_l + \lambda} \quad (9)$$

where G_l and H_l represent sum of gradients and sum of hessians in leaf l, λ represent overfitting parameter.

6. Results & discussion

The yield for the prepared biochar (TW3, TW5, and TW7) was found to be ~40%. The pH of the water suspension of biochar was found to be 8. The characterization and adsorption results are as mentioned below.

6.1. Functional group analysis

A knowledge about the different functional groups present on the adsorbent surface provides a better understanding of the characteristic of the material and how it will interact with the analyte. Fig. 1 shows the FTIR of TW, TW3, TW5, and TW7. TW is majorly composed of lignin, cellulose, hemicellulose, and has polyphenols, carboxylic acid, and amino acids as major functional groups.[41] TW shows the characteristic peak of –O–H stretching (3301 cm^{-1}), C–H stretching in cellulose, hemicellulose and lignin (2845 and 2916 cm^{-1}), C=O or C–O stretching (1640 cm^{-1} and 1029 cm^{-1}), and N–H stretching (1539 cm^{-1}), confirming the presence of above-mentioned functional groups.[42,43] The disappearance of all the characteristic peaks of TW except 1029 cm^{-1} in the FT-IR spectra of biochar confirms the thermal degradation of TW. The peak at 568 cm^{-1} assigned to C–OH bending, 1456 cm^{-1} and 1409 cm^{-1} and 874 cm^{-1} related to the C–H stretching and aromatic nature of biochar was found in all the biochars.[44,45] Thus, the biochar is found to have more in aromatic character as compared to the biomass used as raw material.[46] However, the peak at 874 cm^{-1} diminishes in TW7, indicating loss in the aromatic nature of

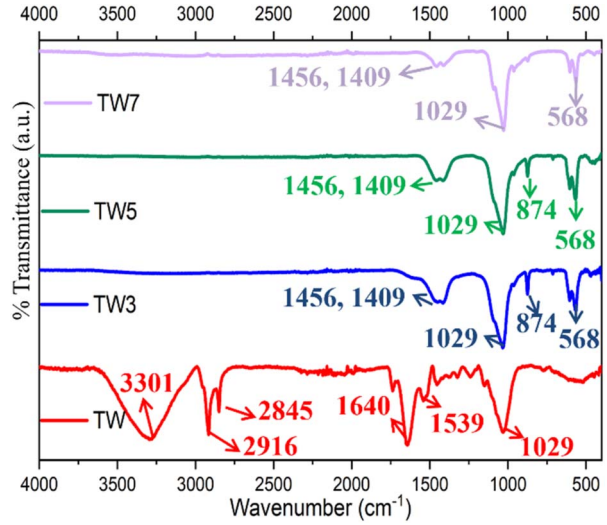

Fig. 1 FTIR of tea waste and prepared biochar samples (TW3, TW5, and TW7).

biochar with rise in decomposition temperature. The aromatic character of biochar provides long-term stability, high surface area, environment for favourable chemical and electrostatic interaction which ensure the enhanced removal of pollutants.[47,48]

6.2. XRD analysis

The XRD spectra of TW and prepared biochar samples is as shown in Fig. 2. From the XRD of TW, a broad peak at 2θ value of 22.3° is observed which indicates the amorphous nature of carbon. As TW is subjected to different temperatures and converted into biochar, sharp peaks are observed. This represents the conversion of amorphous carbon of TW to crystalline carbon in TW3, TW5, and TW7. Peaks corresponding to SiO_2, Fe_2O_3, Fe_3O_4, MnO_2, and Al_2O_3 are found in TW3, TW5, and TW7. Their 2θ values are as marked in Fig. 2b. Additional peaks corresponding to $CaCO_3$ at 31.7° and 39.8° and Al_2O_3 at 25.6° and 46.6° are observed in TW7. All these peaks are matched according to JCPDS no: 44-0141, 82-1533, 33-0664, 39-1346, 05-0586, 10-0173, and 11-0517. The occurrence of these oxides hint towards the presence of ash in biochar samples. From the XRD analysis, we can infer that the ash content increases in biochar when the temperature rises from 300 °C to 700 °C. The increase in ash content might negatively impact the adsorption efficiency as it decreases the available surface area for adsorption. Similar findings have been reported by Tomczyk *et al.*, Loebsack *et al.*, and Hou *et al.*[49–51]

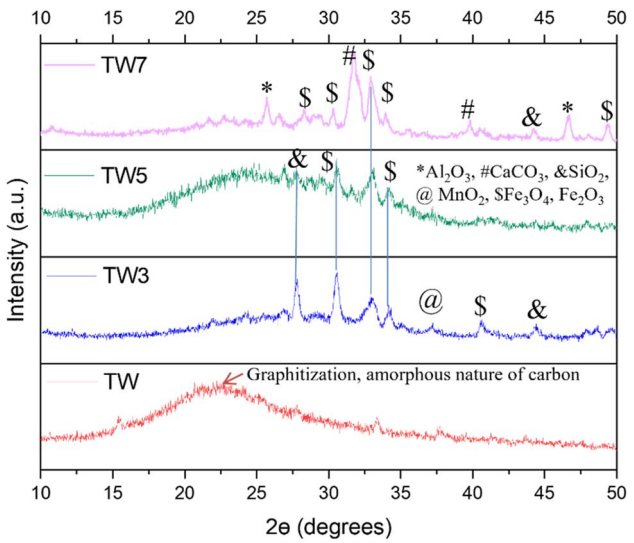

Fig. 2 XRD of tea waste and prepared biochar samples (TW3, TW5, and TW7).

6.3. Surface morphology analysis

From the FE-SEM image of TW (Fig. 3a), it is observed that it has an irregular bumpy heterogenous surface with coarser structure.[52] On subjecting the biomass (TW) to various pyrolysis temperature and conversion to biochar, biochars with different morphologies are formed. This is due to the decomposition and volatilization of matter occurring during pyrolysis process. During the preparation of TW3 and TW5 at 300 °C and 500 °C, the larger particles of TW disintegrate into smaller particles (Fig. 3b and c respectively). TW3 has smaller particles compared to TW5. The disintegration and cracking of TW particles can be attributed to the release of volatile matter.[53] A further increase in the pyrolysis temperature to 700 °C, leads to aggregations of particles in TW7 (Fig. 3d).

6.4. BET analysis

The samples were analysed using BET characterization technique for estimation of surface area and pore size. The BET surface area for TW, TW3, TW5, and TW7 was found to be 6.018 $m^2\ g^{-1}$, 10.653 $m^2\ g^{-1}$, 9.981 $m^2\ g^{-1}$, and 5.734 $m^2\ g^{-1}$. The surface area was noted to increase when TW was converted to TW3 and TW5. This can be related to the fact that the pore-blocking substances (lignin, cellulose, *etc.*) are thermally cracked when subjected to high temperatures.[49,54] However, at 700 °C the surface area decreased to a value even less than TW. This can be to the agglomeration of particles at higher temperatures which is also in accordance with the FE-SEM images. Kumar *et al.*, co-related the decrease in surface area with increase in temperature higher than 600 °C with the structural ordering and pore melting.[55] Owing to the thermal breaking of hemicellulose, lignin, starch, *etc.* and loss of water during the pyrolysis process, pores of different sizes are formed on biochar.[56] TW, TW3, TW5, and TW7 exhibited a pore size of 8.936 nm, 9.204 nm, 9.594 nm, 10.492 nm. This continuous increment in the pore size value with pyrolysis temperature can be related to the release of volatile matter.[57,58]

6.5. Point of zero charge (PZC)

The PZC of the adsorbent is the value of pH at which it bears no net charge on its surface. The PZC value of any material is used for identifying the charge on its surface at a particular pH value. For values of pH less than PZC, the surface of the adsorbent has

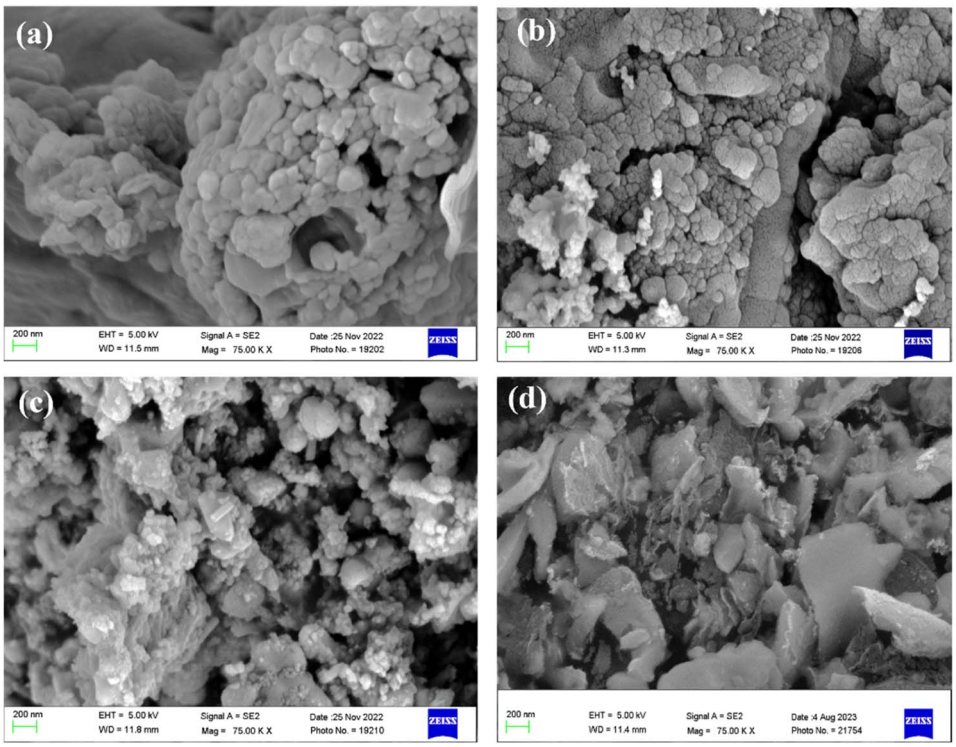

Fig. 3 FE-SEM images of (a) TW, and derived biochar (b) TW3, (c) TW5, and (d) TW7.

a positive charge, indicating the dominance of positively charged adsorbent sites. The adsorbent's surface possesses a negative charge when the value of pH is more than its PZC value. This suggests an increase and governance of negatively charged sites in the adsorption process at pH > PZC. Thus, the PZC analysis plays a vital role in deciphering the adsorption mechanism. For TW, the PZC value was found to be 6.6 (Fig. 4a). As the biomass (TW) is converted into biochar the PZC value is noted to be increasing. For TW3, TW5, and TW7 the PZC was calculated to be 7.3, 7.5 and 8.3 respectively (Fig. 4b–d). From this we can conclude that as the pyrolysis temperature increases from 300 °C to 700 °C, the PZC value also rises. This property

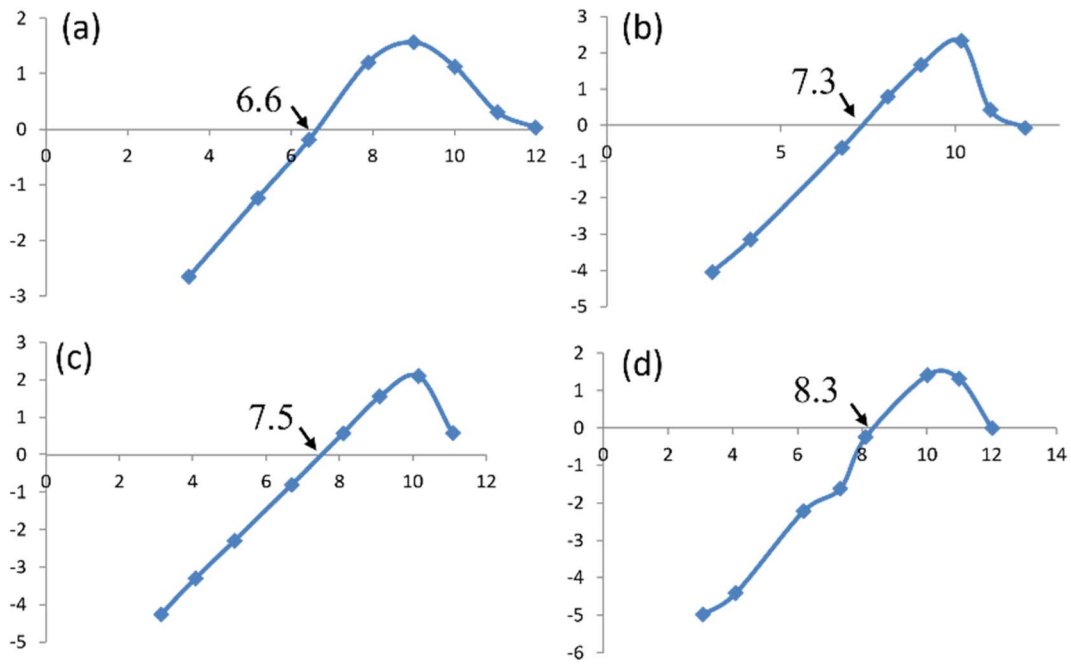

Fig. 4 Point of zero charge of (a) TW, and derived biochar (b) TW3, (c) TW5, and (d) TW7 using salt addition method.

Table 2 Removal (%) of pollutants using tea waste and its biochars

Code	CPY	4-NA	MG	CR
TW	45.28	0	92.84	38.63
TW3	48.81	18.08	83.82	46.34
TW5	50.89	0	83.43	80.78
TW7	50.36	0	97.35	84.61

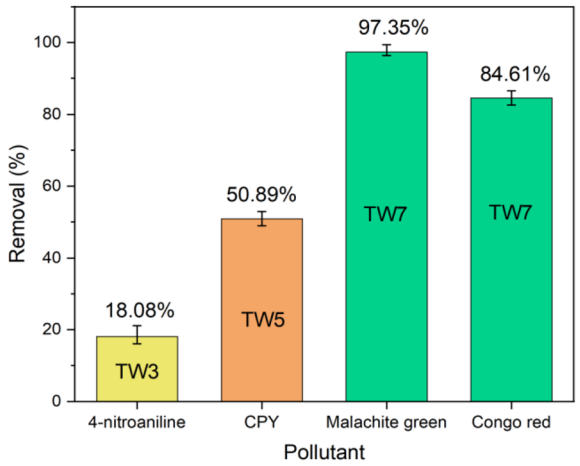

Fig. 5 Graphical representation of the most effective adsorbent for removal of different pollutants and their removal % (conc. of analyte = 10 ppm, adsorbent dosage = 1 mg ml^{-1}, 60 min).

can be associated with the release of alkaline salts at higher temperature.[59]

6.6. Adsorption studies

6.6.1. Individual adsorption studies. TW, TW3, TW5, and TW7 were evaluated for the individual removal of CPY, 4-NA, MG, and CR. The % removal values of all the pollutants are as shown in Table 2. As observed from the results, only TW3 showed removal of 4-NA (18.08%). CPY was best removed by TW5 (50.89%), while TW7 was the most effective for dye removal *i.e.* MG (97.35%) and CR (84.61%). These findings have been graphically represented in Fig. 5.

The hydrophobicity of the biochar is said to be increasing along with the rise in pyrolysis temperature. The hydrophobic character of the biochar is reported to be favourable for the adsorption of agrochemical.[60] So, increase in hydrophobicity with increase in temperature from 300 to 700 °C could be the reason for higher adsorption of CPY on TW5 and TW7 as compared to TW3. Similar findings have been reported by Zhang *et al.*, where hydrophobicity of biochar has promoted the adsorption of different organophosphorus insecticides. The adsorption of 4-NA, is likely to be facilitated by the more oxygen rich functional groups of the biochar pyrolyzed at lower temperature like 300 °C (TW3) in comparison to that at higher temperatures such as 500 °C-900 °C (TW5 and TW7).[61] In case of dye adsorption, an adsorbent with greater pore size benefits the process as large pores are required to accommodate bulky dye molecules.[62,63] TW7 has the largest pore size as compared to other studied materials in the study (as estimated by BET analysis), resulting in its highest dye removal efficiency.

6.6.2. Simultaneous removal studies. After primary evaluation from the individual adsorption studies, a detailed simultaneous removal of pollutants from synthetic wastewater was carried out. All the three biochar samples (TW3, TW5, and TW7) were further investigated for their potential in removal of pollutants from a mixture of agrochemical, aromatic molecule, and industrial dyes (CPY, 4-NA, MG, and CR). It was calculated that TW3, TW5, and TW7 showed an overall removal percentage of 49.65 ± 3, 53.45 ± 2, and 47.48 ± 2, respectively in 60 min. The individual removal of each component is as mentioned in Table S2 (ESI).† From the results, it can be concluded that TW5

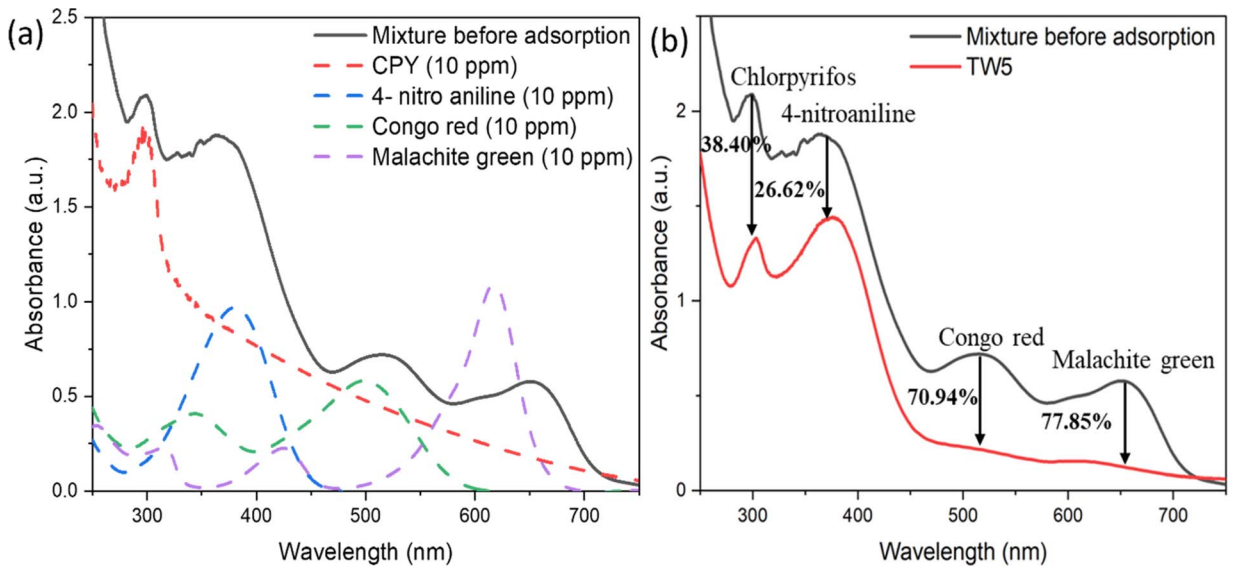

Fig. 6 UV-visible graph of (a) synthetic wastewater mixture and individual analyte before adsorption, and (b) simultaneous adsorption of pollutants from synthetic wastewater by TW5 (conc. of analyte = 40 ppm, adsorbent dosage = 1 mg ml^{-1}, 60 min).

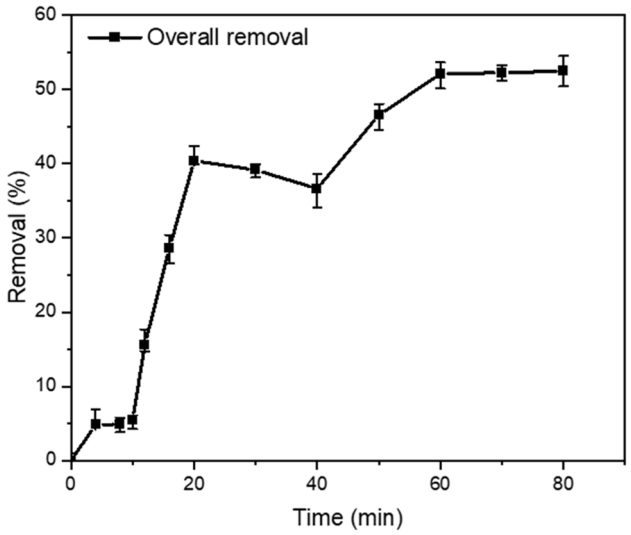

Fig. 7 Overall removal % from synthetic wastewater with respect to time by TW5 (conc. of synthetic wastewater = 40 ppm, pH = 7, adsorbent dosage = 1 mg ml^{-1}, time = 80 min).

was the most efficient adsorbent for simultaneous removal. Fig. 6a and b shows the UV-visible spectra for the adsorption of mixture using TW5. Thus, TW5 was further assessed by performing the kinetic, dosage and pH study for the simultaneous adsorption.

6.6.2.1. Kinetic studies. For the kinetic study, the concentration of the mixture was monitored at every 10 min (4 min during the rapid adsorption stage *i.e.* till 20 min) till 60 min as saturation was observed post 60 min (Fig. 7). A slight drop in removal efficiency was observed at 30 and 40 minutes, which could be attributed to temporary desorption. This desorption can be attributed to the redistribution of adsorbate, surface reorganization, or weakly/reversibly bound molecules being temporarily released during the adsorption process. At the end of 60 min, 52.16 ± 2% of overall removal was achieved from the mixture. Based on the kinetic data, different kinetic models namely first order (FO), second order (SO), pseudo first order (PFO), pseudo second order (PSO), Elovich, and intra-particle diffusion were plotted (according to their linear equations) to get a better understanding of the nature of the adsorption process (Fig. 8a–f). The overall Q_e value was found to be 4.58 mg g^{-1}. The value of individual Q_e, K, and R^2 for each pollutant derived from the linear fitting of the kinetic models are mentioned in Table S3.† From the comparative high value of R^2 of second order graph, we can conclude that the reaction follows second order kinetics. This suggests that the adsorption process is dependent on the concentration of analyte and number of active adsorbent sites.

6.6.2.2. Effect of adsorbent dosage. The dosage studies were performed for identification of the optimal dosage of adsorbent (TW5) for maximum removal efficiency. The bar graph showing the overall % removal at varying dosage is as shown in Fig. 9. The % removal of individual component and overall adsorption is summarized in Table S4.† On increasing the dosage from 0.1 mg ml^{-1} to 5 mg ml^{-1}, the overall removal efficiency was found to increase from 9.32 ± 2% to 81.39 ± 2.1%. The enhancement in the removal (%) can be due to the increasing availability of adsorption sites with increasing dosage of TW5.

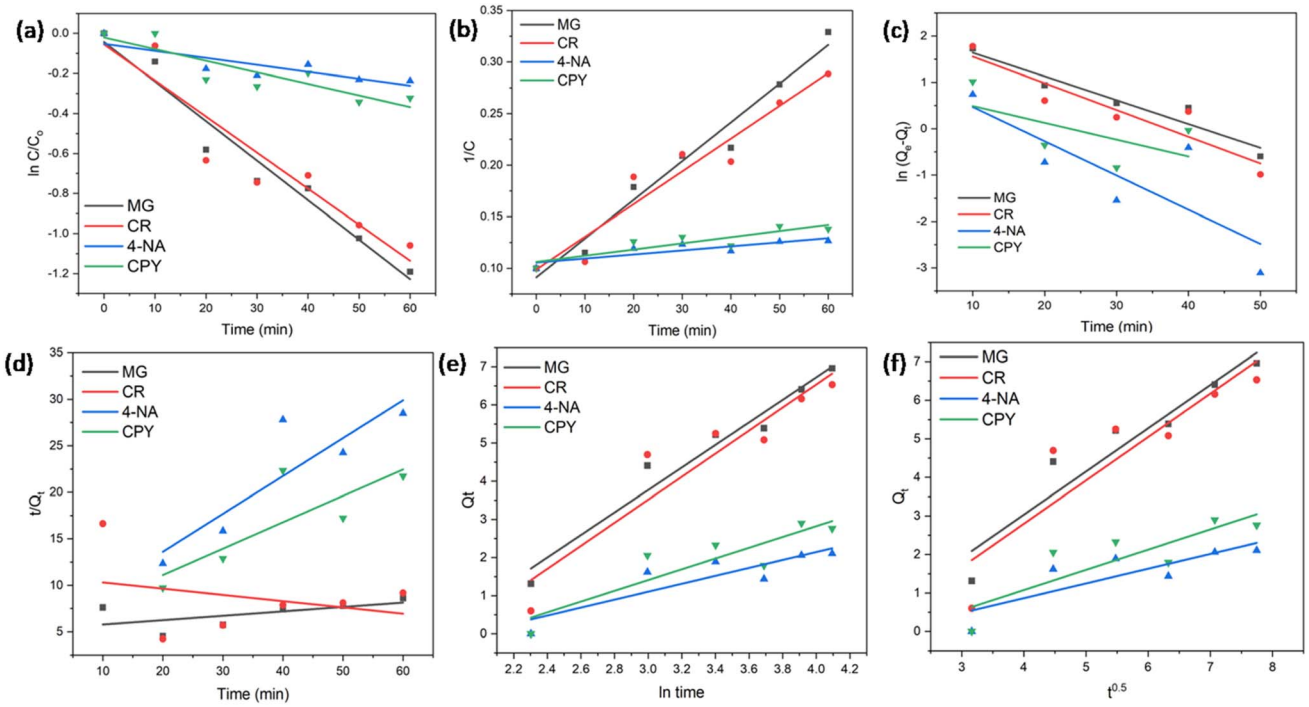

Fig. 8 Linear fitting of (a) first order, (b) second order, (c) Pseudo first order, (d) Pseudo second order, (e) Elovich, and (f) intra-particle diffusion models for simultaneous removal by TW5.

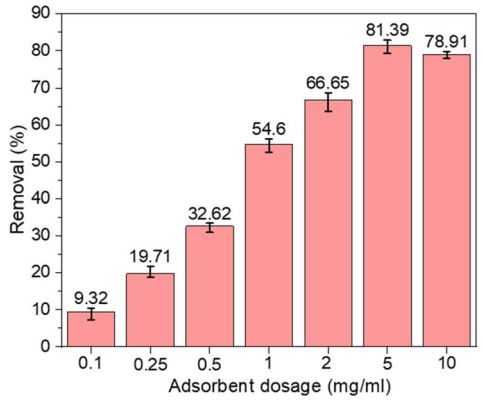

Fig. 9 Overall removal (%) of the mixture at different TW5 dosage (conc. of synthetic wastewater = 40 ppm, pH = 7, adsorbent dosage = 0.1 to 10 mg ml^{-1}, time = 60 min).

At adsorbent dosage of 10 mg ml^{-1}, a decrease in the efficiency was noted. This may be due to the agglomeration of particles. Similar results have been reported in several studies.[64,65]

6.6.2.3. Effect of pH of analyte. The basicity and acidity of the analyte solution highly affects the characteristic of the analyte and the adsorbent, thus influencing the adsorption process. Various factors like charge, structure, chemical and physical properties get affected with a change in pH of the solution which in turn influences the interaction between the adsorbent and analyte. For the study, the pH of the analyte solution was adjusted as described in section 4. The pH of the aqueous solution was found to be 7. The UV-visible graph is as shown in Fig. 10a and the bar graph for overall removal (%) is as shown in Fig. 10b. The individual removal (%) of each pollutant at different pH are summarized in Table S5.† A highest overall removal of 62.72 ± 0.9% was obtained at pH value of 2, which decreased to ~45% as the pH increased from 2 to 12. MG shows maximum removal of 89% at extremely high basic (pH 12) medium. Maximum adsorption of CR was observed at highly acidic pH of 2 (77.22%), which decreased with increasing value of pH, attaining its minimum value of 47.92% at pH 12. At the pH of 2, 32.99% of 4-NA was adsorbed, while at the pH value of 4 and 7, there was a slight drop of 7% in the removal of 4-NA which decreases furthermore at pH of 12 (15.90%). For CPY, the removal % was found to be gradually decreasing from 53.90% (at pH = 2), to 27.37% (at pH = 12). Further discussion regarding the nature of adsorption at the studied pH is as mentioned in section 5.4 (mechanism of adsorption). The results obtained from dosage and pH studies, infer that maximum overall removal can be achieved at 5 mg ml^{-1} of adsorbent dosage and pH 2. Thus, a maximum overall removal of 82.66 ± 1.3% was obtained for the treatment of synthetic wastewater at pH 2 and 5 mg ml^{-1} dosage of TW5.

6.6.2.4. Effect of concentration of analyte. The bar chart as shown in Fig. 11 displays the efficacy of contaminant removal (%) at various analyte concentrations (5, 10, 20, and 40 mg L^{-1}). The removal (%) of each component in the mixture dye is as mentioned in Table S6.† The highest clearance efficiency was recorded at 10 mg L^{-1} (61.76 ± 2.8%), closely followed by 5 mg L^{-1} (60.55 ± 2.3%). When the analyte concentration increased to 20 mg L^{-1}, the removal efficiency somewhat decreased to 59.5 ± 1.9%, but it became more apparent at 40 mg L^{-1}, when it dropped to 50.33 ± 1.1%. This graph demonstrates that as the analyte concentration increases over a certain threshold, the adsorption efficacy decreases because the surface of the biochar has reached saturation of available adsorption sites. These findings highlight the need of optimizing operational parameters for effective wastewater treatment and show how analyte concentration influences removal performance.

6.6.2.5. Effect of temperature. On varying the temperature of the adsorption system, the removal (%) was found to be 28.15%, 29.69%, 53.85%, 42.31%, and 41.08% at 278 K, 288 K, 298 K, 318 K, and 323 K, respectively. From the removal (%) values, it can

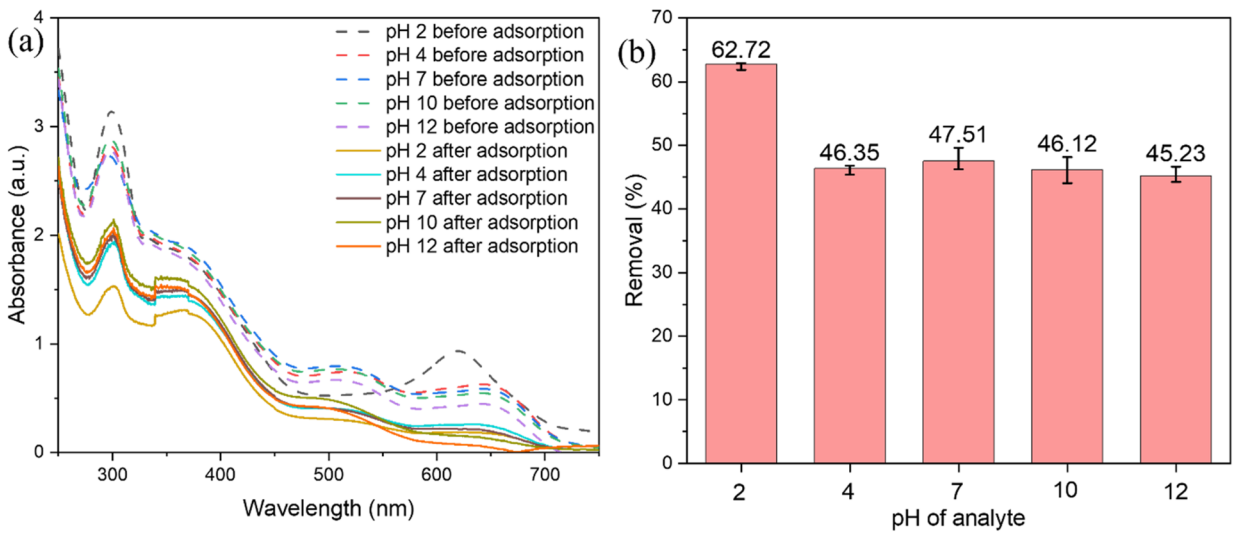

Fig. 10 (a) UV-visible graph, and (b) bar graph showing the removal of pollutants from the mixture at different pH values of the analyte solution (conc. of synthetic wastewater = 40 ppm, pH = 2 to 12, adsorbent dosage = 1 mg ml^{-1}, time = 60 min).

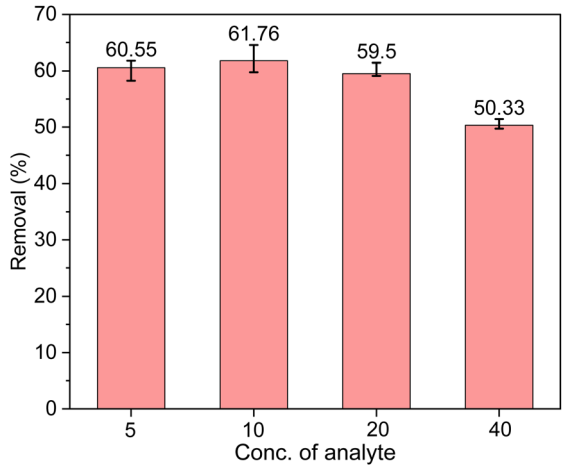

Fig. 11 Bar graph showing the overall removal (%) of pollutants at different analyte concentrations (conc. of analyte = 5–40 ppm, pH = 7, adsorbent dosage = 1 mg ml^{-1}, time = 60 min).

be said that high temperature favoured the reaction process as compared to decreased at low temperatures. Highest efficiency was recorded at room temperature, depicting the optimum temperature condition (298 K). The obtained experimental data was fitted into eqn (10), to obtain the value of ΔG. The obtained ΔG was used to plot the graph of ΔG *versus* temperature (K) according to eqn (11).

$$\Delta G = -RT \ln k \quad (10)$$

$$\Delta G = \Delta H - T\Delta S \quad (11)$$

where, ΔG = change in Gibbs free energy, R = gas constant (8.314 J mol^{-1} K^{-1}), T = temperature (Kelvin), k = solute coefficient ($1000Q_e/C_e$), ΔH = change in enthalpy, ΔS = change in entropy.

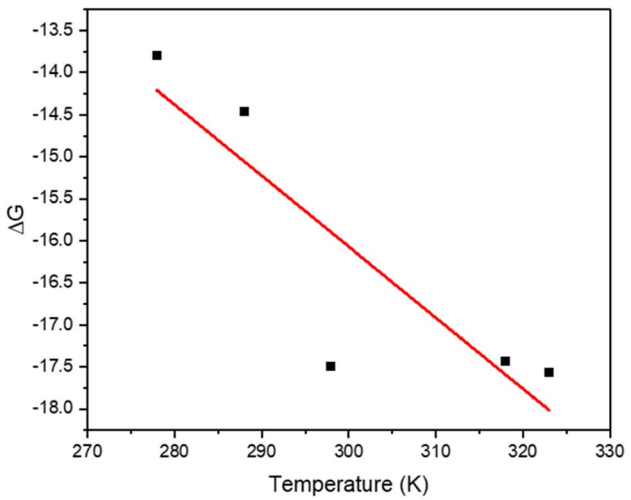

Fig. 12 Thermodynamic plot for overall removal (conc. of analyte = 40 ppm, adsorbent dosage = 1 mg ml^{-1}, time = 60 min, temperature = 278 K, 288 K, 298 K, 318 K, and 323 K).

Fig. 12 shows the plotted graph of ΔG *versus* temperature (K). The negative values of ΔG (kJ mol^{-1} K^{-1}) indicates the spontaneous nature of the adsorption process at all temperature. The values of ΔS and ΔH were found to be 0.0844 J mol^{-1} K^{-1} and 9.276 kJ mol^{-1}, respectively as derived from the graph. The positive value of ΔS corresponds to the increase in entropy/randomness of the system, while the positive value of ΔH hints towards the endothermic nature of adsorption process.

6.7. Mechanism of adsorption

The mechanism is profoundly dependent on the charge of the analyte and adsorbent, their functionalities, charge, and porosity of the adsorbent, which in turn determines the nature of interaction between them. Various interactions like π–π interaction, hydrophobic interactions, hydrogen bonding, and pore-filling are involved in the adsorption of pollutants. The aromatic functional groups present in MG, CR, CPY, and 4-NA can act as π-electron acceptors while the aromatic rings in TW5 may act as π-electron donors. This results in the adsorption of pollutant *via* π–π interaction. The hydrophobic groups like alkyl chains, methyl groups, *etc.* present in the analyte and adsorbent allow the removal of pollutant through hydrophobic interactions. Oxygen and nitrogen like atoms present in the analyte forms hydrogen bonds with functional groups like –OH, and –COOH present on the surface of TW5, facilitating their adsorption. The porous network and surface area of TW5 allow the diffusion of the pollutants in the pores resulting in their removal from the aqueous solution.

As per the results obtained from the pH studies (Table S5† and Fig. 10) and PZC of TW5, a plausible mechanism for the adsorption of each pollutant (based on the charge) from the synthetic wastewater is discussed (Fig. 13). The PZC value of TW5 is 7.5 as identified from the PZC analysis, implying that for pH values <7.5, the adsorbent's surface is positively charged, while for pH values >7.5, it is negatively charged. Ion-exchange interactions between like charges of analyte and adsorbent are responsible for the adsorption of positively charged pollutant, that is MG from the studied synthetic wastewater in the acidic medium. In the basic medium, the adsorptive removal process is governed by electrostatic attraction amongst positive MG and negative TW5.[66] The adsorption of negatively charged CR, 4-NA, and CPY is facilitated in the acidic medium owing to electrostatic interactions between negative charges of the pollutants and positively charged adsorbent. As the pH increases and shifts to basic, a decrement in removal % is observed for the negatively charged pollutants due to the electrostatic repulsion between the like charges of analyte and adsorbent.[67–69]

6.8. Column filtration adsorption study

From the conducted (effect of analyte) study, it was observed that better removal efficiency is achieved at 10 ppm concentration of the analyte. Therefore, with an aim to develop a portable filter for wastewater treatment, the present study was scaled up *via* column adsorption process for adsorption of 10 ppm analyte solution. The bar chart (Fig. 14) displays the pollutants' removal efficacy (%) at different combination

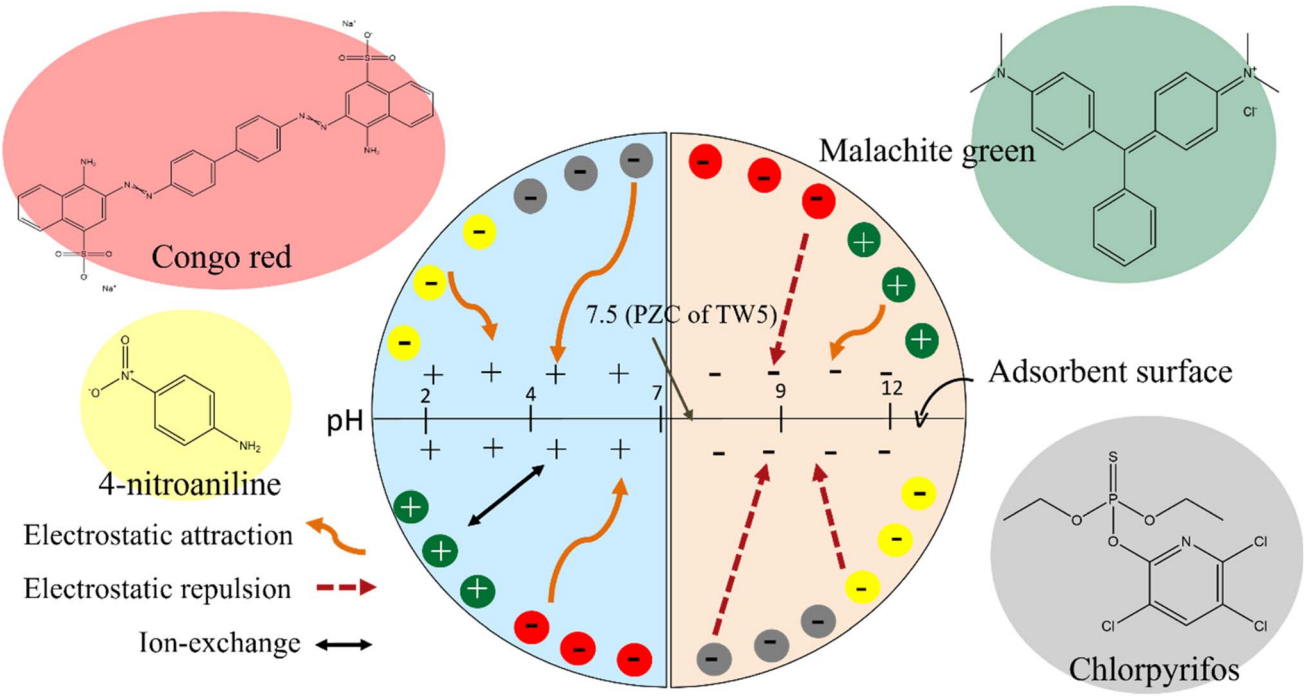

Fig. 13 Mechanism of adsorption of pollutants during their simultaneous removal at different acidic and basic pH values.

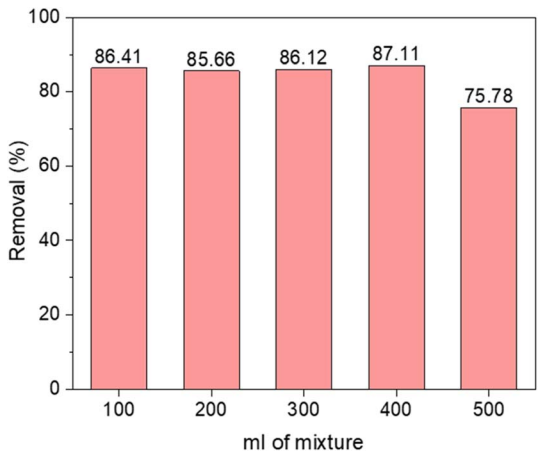

Fig. 14 Bar graph showing the overall removal (%) of mixture by column filtration study.

volumes (100 to 500 ml). The % removal of the individual components for every 100 ml solution is as mentioned in Table S7.† The elimination efficiency peaked at 400 ml (87.11%), with 100 ml (86.41%) and 300 ml (86.12%) following closely after. The removal efficiency dropped somewhat to 85.66% at 200 ml, but it dropped dramatically to 75.78% at 500 ml. The statistics demonstrate that the adsorbent is considerable efficient within a certain volume range; beyond this range may lower the number of accessible adsorption zones or dilute the pollutant concentration, both of which would reduce efficacy. These findings demonstrate how important it is to maintain the mixture volume at the optimal amount for optimal removal efficacy.

6.9. Recyclability of spent adsorbent

The bar chart in Fig. 15 depicts the removal efficacy (%) of pollutants across five adsorption–desorption cycles and the individual removal is as mentioned in Table S8.† With a removal efficiency of 53.45 ± 2.1%, the first cycle retained the greatest performance. However, a continuous decline in removal efficiency was seen with each cycle. In the second and third cycles, the efficiencies dropped slightly to 51.13 ± 1.8% and 52.47 ± 2.3%, respectively. In the fourth cycle, the removal efficiency dropped to 40.98 ± 0.8%, and in the fifth cycle, it dropped to 32.75 ± 2.2% once again. This trend suggests that with repeated usage, the adsorbent's capacity to remove pollutants gradually decreases, most likely due to the loss or saturation of active adsorption sites. These results emphasize the need of further investigation into adsorbent regeneration techniques to sustain high removal efficiencies across many cycles.

The adsorbent after adsorption and regeneration was characterized using FTIR to study the nature of adsorption and stability of adsorbent post-regeneration, Fig. 16 shows the FTIR spectra of TW5 before adsorption, after adsorption, and after regeneration. On comparing the spectra of TW5 before and after adsorption, disappearance of peaks and appearance of new peaks is observed post-adsorption. This suggests the vital role of functional groups of adsorbents in the adsorption of pollutants. The disappearance of peaks attributed to aromatic character of biochar (C–C stretching in aromatic ring), C=C stretching, symmetric COO– stretching can be due to electrostatic

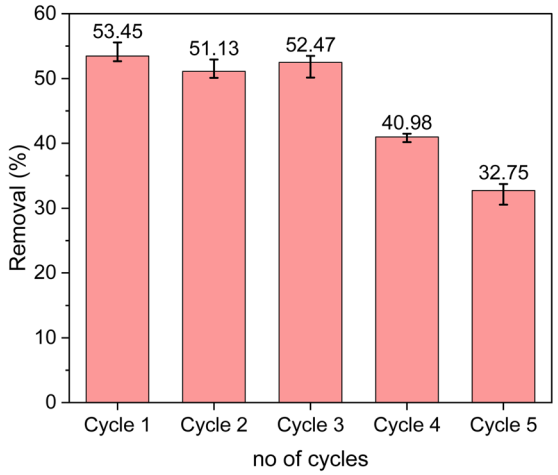

Fig. 15 Bar graph of overall removal of pollutants from the mixture during different cycles of TW5 (conc. of synthetic wastewater = 40 ppm, pH = 7, adsorbent dosage = 1 mg ml^{-1}, time = 60 min).

attraction between dye and functional groups, π–π interactions, hydrophobic interaction and hydrogen bonding. New peaks at 957 cm^{-1}, 915 cm^{-1}, and 533 cm^{-1}, are observed in FTIR spectrum after adsorption. The peaks at 957 cm^{-1} and 915 cm^{-1} represents the C=C of alkenes and C–H out of plane vibration. These peaks can also be due to the vibrations relating to phosphate group of chlorpyrifos, aromatic amines possibly from 4-NA. The peak at 533 cm^{-1} is associated with metal-oxide bond. For the present study, this peak can be due to the formation of Si–O or Fe–O bond between minerals/metal-oxides in biochar and oxygen containing functional groups of pollutant. The spectrum of TW5 after regeneration with acetone shows similar peaks as after adsorption spectrum, suggesting that chemical bonds are formed between pollutant and adsorbent and thus are not broken by acetone. However, in the recyclability study of TW5 it is observed that the adsorbent shows good performance for up to 3 cycles. This suggests that acetone has freed up the active adsorption sites and pores without altering the chemical bonds.

6.10. Machine learning prediction

The present study extensively investigated the adsorption capacities of the tea waste-derived biochar across a range of synthesis and operation conditions. The % removal efficiency was predicted using two advanced machine learning models, RNN and CatBoost, additionally with and without Bayesian optimization. The performance of these models was rigorously assessed, and their prediction accuracy and reliability were thoroughly reviewed, using three crucial evaluation metrics: R^2, MAE, and RMSE. It is clear from Fig. 17a, that during the training phase, CatBoost R^2 value of 0.99 was a significant increase of around 28.17% when compared to RNN R^2 value of 0.77. This indicates the underlying patterns in the efficacy of pollutant removal and shows how well CatBoost matches the training data. Similarly, CatBoost achieved an R^2 value of 0.91 during the ten-fold cross-validation phase, outperforming RNN by 26.68%. This improvement demonstrates how CatBoost improves training performance and generalizes to new data efficiently, reducing the likelihood of overfitting. The results demonstrate how reliable and robust CatBoost is in simulating the efficacy of pollution removal, making it a superior choice for this study than RNN. As observed from Fig. 17b, during the training phase, CatBoost performed about 89.18% better than RNN, which had an MAE of 11.23, with an MAE of 1.21. This illustrates CatBoost remarkable ability to lower training prediction errors, ensuring a more accurate match with actual values. Similarly, during the ten-fold cross-validation phase, CatBoost MAE of 5.62 was about 52.85% lower than RNN' MAE

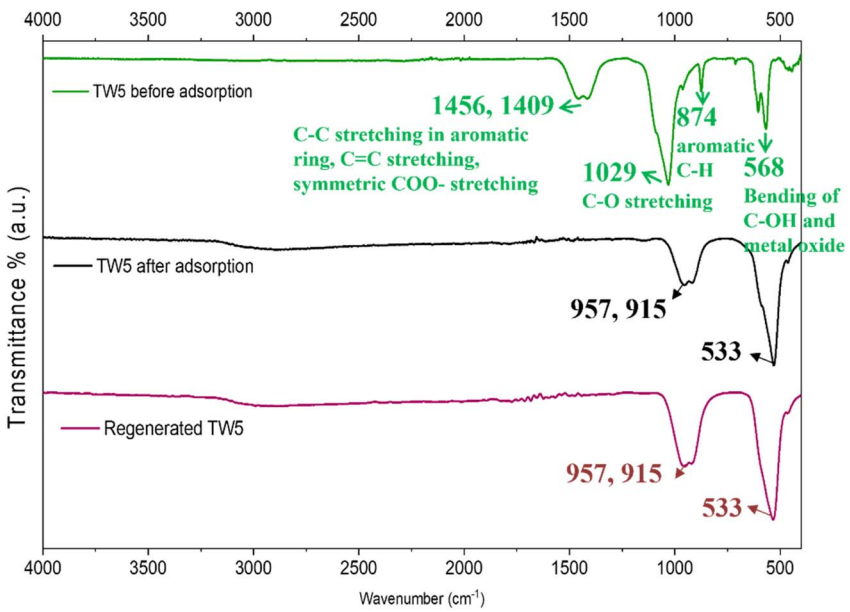

Fig. 16 FTIR spectra of TW5 before adsorption, after adsorption, and after regeneration.

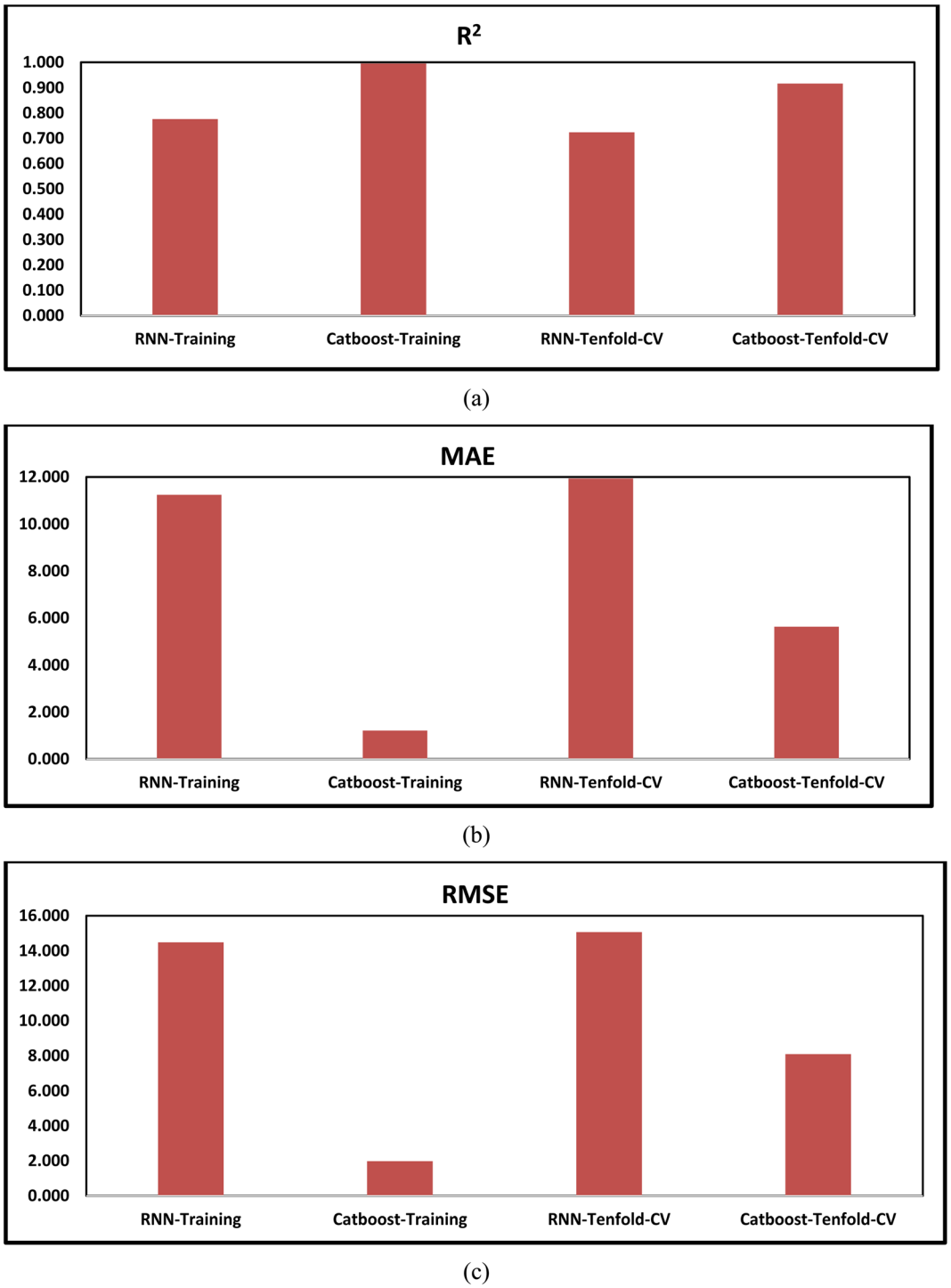

Fig. 17 Prediction results of (a) R^2, (b) MAE, and (c) RMSE from ML models without optimization.

of 11.93. This reduction illustrates CatBoost enhanced ability to generalize and maintain low prediction errors across unknown inputs. While performing training and ten-fold cross-validation on the experimental dataset, it is observed from Fig. 17c, CatBoost outperformed RNN, based on the comparative study of RMSE values obtained. The RMSE of value of 1.97 obtained during training of CatBoost is around 86.35% lower than the RMSE value of 14.48 for RNN. This significant decrease suggests that CatBoost can model the data with much lower prediction errors, leading to improved accuracy in the training stage. CatBoost RMSE of 8.09 during the ten-fold cross-validation phase was 46.28% lower than RNN's RMSE of 15.07. This illustrates how well CatBoost generalizes, guaranteeing more reliable results on unknown datasets.

As observed from Fig. 18a, the analysis of R^2 values obtained when ML models are optimized with Bayesian optimization

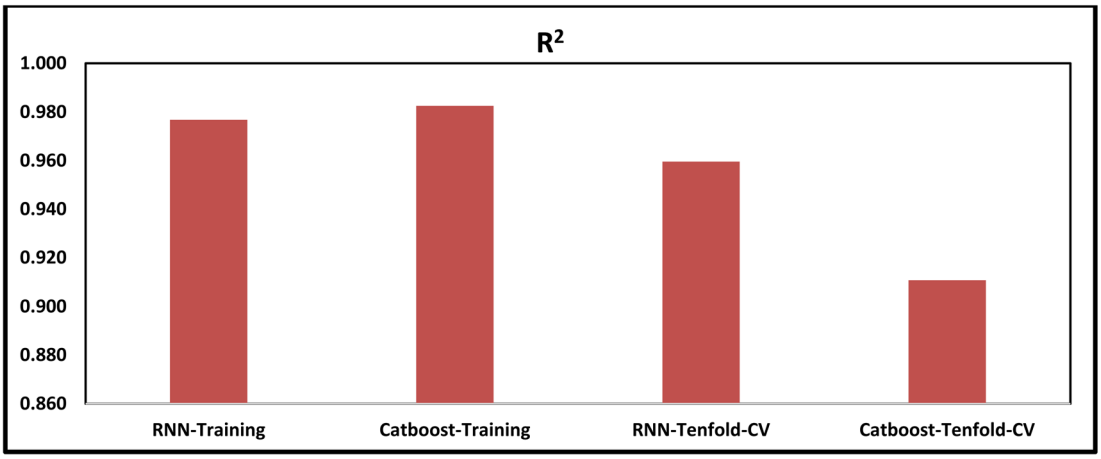

(a)

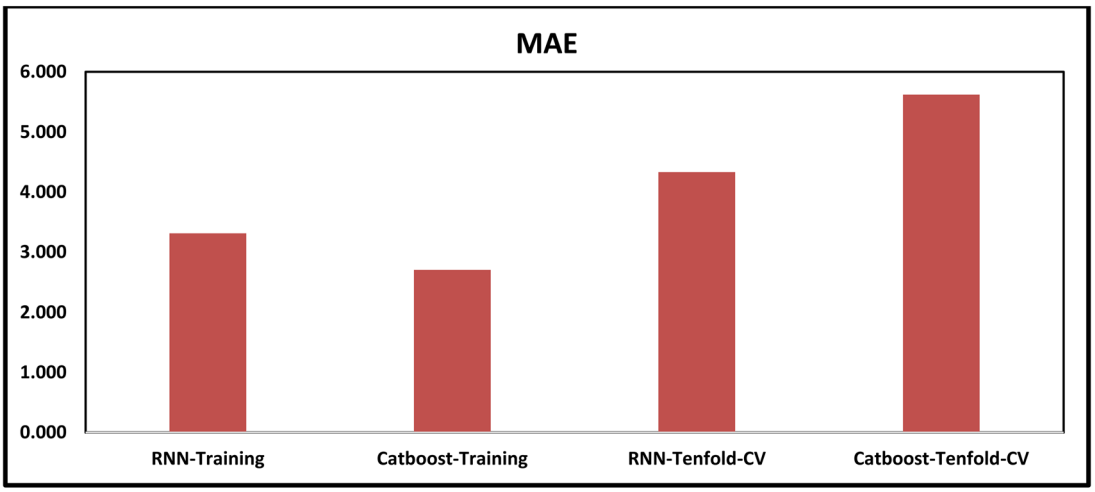

(b)

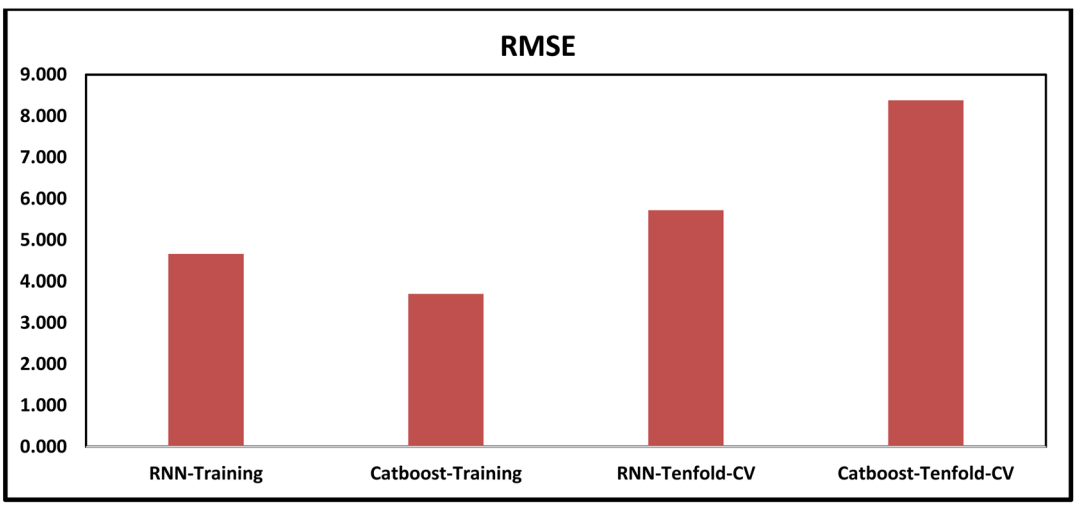

(c)

Fig. 18 Prediction results of (a) R^2, (b) MAE, and (c) RMSE from ML models with Bayesian optimization.

demonstrates the impact of hyperparameter modification on the prediction of % removal. During the training phase, RNN and CatBoost both demonstrated exceptional accuracy with R^2 values of 0.977 and 0.983, respectively. When compared to RNN, CatBoost R^2 increased by 0.61%, suggesting that Bayesian optimization was effective in modifying CatBoost

hyperparameters, enhancing its capacity to detect complex relationships in the data. During the ten-fold cross-validation phase, the RNN R^2 score of 0.960 was about 5.10% more than CatBoost R^2 value of 0.911. This implies that even though both models shown exceptional performance during training, RNN maintained a higher generalization ability on unknown data after Bayesian optimization. The investigation of MAE values after Bayesian optimization indicates the meaningful differences in prediction capabilities between RNN and CatBoost models as observed from Fig. 18b. CatBoost achieved a drop of around 18.35% throughout the training phase, with a lower MAE of 2.705 than RNN's MAE of 3.314. This implies that after optimization, CatBoost was better able to find correlations in the training data and minimize errors. During the ten-fold cross-validation phase, RNN demonstrated better generalization with a lower MAE of 4.333 than CatBoost MAE of 5.619, indicating a 22.88% relative improvement. This suggests that RNN beat CatBoost on unknown data, even though CatBoost did quite well in training accuracy. The RMSE values (Fig. 18c) after Bayesian optimization clearly demonstrate performance trends between the RNN and CatBoost models. When compared to RNN 4.660, CatBoost showed a drop of around 20.55% throughout the training phase, with a lower RMSE of 3.703. This implies that CatBoost was better at finding patterns in the data and lowering prediction errors during training. Moreover, in the ten-fold cross-validation stage, RNN performed reasonably better than CatBoost, with an RMSE of 5.721, which was 31.69% lower than CatBoost RMSE of 8.377. The prediction results shows that RNN has better generalization capabilities than CatBoost, making it more reliable on unknown data.

7. Conclusion

This study investigates the simultaneous removal of multiple organic pollutants, notably malachite green, congo red, 4-nitroaniline, and chlorpyrifos, utilizing biochar derived from tea waste. The optimal adsorbent (TW5) was evaluated under a number of conditions, including pH, concentration, dosage, contact time, and temperature. Under optimal conditions, which included a pH of 2, a contact period of 60 minutes, and an adsorbent dose of 5 mg ml^{-1}, a maximum removal efficiency of 82.66% was observed. The adsorption procedure corresponded to second-order kinetic models, which offered a solid justification for the mechanism of pollutant removal. The portable column filtration device demonstrated its value in real-time wastewater treatment by eliminating 90% of coexisting pollutants. ML models were applied to the experimental data set to predict the adsorption efficiency. With reduced MAE and RMSE values throughout both the training and cross-validation stages, RNN was shown to be the most effective model for % removal prediction. Although CatBoost performed well during training, its generalization was less reliable. These findings show that it is possible to enhance pollutant removal processes by fusing state-of-the-art machine learning techniques with experimental insights, offering a workable and reasonably priced choice for wastewater treatment applications.

Although the present work evaluates biochar as an adsorbent for multi-component system, other pollutants like oil, heavy metals, surfactants, *etc.* present in the wastewater can alter the adsorption performance of the adsorbent. The separation of the adsorbent is another challenge that can surface during the real-time wastewater analysis. Considering the drawbacks, several modification/functionalization techniques like acid modification, base modification, and magnetization can be used to develop adsorbent with enhanced efficiency and easy separation post-adsorption. A membrane fabrication can be attempted to convert the presented work into a more applicable and feasible form for large-scale wastewater treatment. ML models can be applied for selecting and analyzing the optimum pyrolysis conditions for biochar preparation to obtain maximum removal efficiency.

Data availability

The authors declare that the data supporting the findings of this study are available within the paper and its ESI files.† Should any raw data files be needed in another format they are available from the corresponding author upon reasonable request.

Author contributions

SJ: data collection, analysis and interpretation of results draft manuscript preparation, VK: software modelling, manuscript preparation, MAM: funding, resources, review and revision of the manuscript, RG & SS: supervision, review and revision of the manuscript, conceptualization. All authors reviewed the results and approved the final version of the manuscript.

Conflicts of interest

The authors declare that they have no known competing financial interests or personal relationships that could have appeared to influence the work reported in this paper.

Acknowledgements

The authors would like to thank Solar Research and development Centre (SRDC) for FE-SEM characterization. The authors would like to thank Pandit Deendayal Energy University, and the Government of Gujarat for the award of research fellowship (KCG/SHODH/2022-23/202101586) under the Scheme for Developing High Quality Research. This work was supported by the Deanship of Scientific Research, Vice Presidency for Graduate Studies and Scientific Research, King Faisal University, Saudi Arabia [Grant No. KFU252589].

References

1 M. Kummu, *et al.*, The world's road to water scarcity: shortage and stress in the 20th century and pathways towards sustainability, *Sci. Rep.*, 2016, **6**(1), 38495.

2 C. Ingrao, *et al.*, Water scarcity in agriculture: An overview of causes, impacts and approaches for reducing the risks, *Heliyon*, 2023, **9**(8), e18507.
3 S. Jahan and A. Singh, Causes and Impact of Industrial Effluents on Receiving Water Bodies: A Review, *Malays. J. Sci. Adv. Technol.*, 2023, **3**(2), 111–121.
4 J. Patel, *et al.*, A Facile One-Pot Approach for Synthesis of Graphene-CdS Nanocomposites and Implementation towards Visible Light Driven Photocatalytic Degradation of Chlorpyrifos (One-Pot Synthesis of G-CdS for the degradation of CPY)**, *ChemistrySelect*, 2024, **9**(2), e202302762.
5 V. Sodha, *et al.*, Synthesis of zeolite-doped polyaniline composite for photocatalytic degradation of methylene blue from aqueous solution, *Environ. Sci. Pollut. Res. Int.*, 2023, **30**(16), 46159–46174.
6 K. H. Hama Aziz, *et al.*, Heavy metal pollution in the aquatic environment: efficient and low-cost removal approaches to eliminate their toxicity: a review, *RSC Adv.*, 2023, **13**(26), 17595–17610.
7 S. Jha, *et al.*, Biochar as Sustainable Alternative and Green Adsorbent for the Remediation of Noxious Pollutants: A Comprehensive Review, *Toxics*, 2023, **11**(2), 117.
8 Z. Darban, *et al.*, Hydrogel-Based Adsorbent Material for the Effective Removal of Heavy Metals from Wastewater: A Comprehensive Review, *Gels*, 2022, **8**(5), 263.
9 F. Younas, *et al.*, Current and Emerging Adsorbent Technologies for Wastewater Treatment: Trends, Limitations, and Environmental Implications, *Water*, 2021, **13**(2), 215.
10 N. Mahfoudhi, Nanocellulose as a novel nanostructured adsorbent for environmental remediation: a review, *Cellulose*, 2017, **24**, 1171–1197.
11 T. A. Aragaw and F. M. Bogale, Biomass-Based Adsorbents for Removal of Dyes From Wastewater: A Review, *Front. Environ. Sci.*, 2021, **9**, 764958.
12 M. Ghaedi, *et al.*, Application of central composite design for simultaneous removal of methylene blue and Pb^{2+} ions by walnut wood activated carbon, *Spectrochim. Acta, Part A*, 2015, **135**, 479–490.
13 S. Marghzari, *et al.*, Simultaneous elimination of Malachite Green, Rhodamine B and Cresol Red from aqueous sample with Sistan sand, optimized by Taguchi L16 and Plackett-Burman experiment design methods, *Chem. Cent. J.*, 2018, **12**(1), 116.
14 P. Xing, *et al.*, Removal of Pb(II) from aqueous solution using a new zeolite-type absorbent: Potassium ore leaching residue, *J. Environ. Chem. Eng.*, 2018, **6**(6), 7138–7143.
15 S. Fan, *et al.*, Biochar prepared from co-pyrolysis of municipal sewage sludge and tea waste for the adsorption of methylene blue from aqueous solutions: Kinetics, isotherm, thermodynamic and mechanism, *J. Mol. Liq.*, 2016, **220**, 432–441.
16 D. Balarak, *et al.*, Studies on the Removal of Amoxicillin by Single Walled Carbon Nanotubes, *Br. J. Pharm. Res.*, 2016, **10**(4), 1–9.
17 N. Memon, *et al.*, Synthesis, Characterization, and Application of Co-Al-Zn Layered Double Hydroxide/Hydrochar Composite for Simultaneous Removal of Cationic and Anionic Dyes, *J. Chem.*, 2021, **2021**(1), 1138493.
18 S. Sultana, *et al.*, Adsorption of crystal violet dye by coconut husk powder: Isotherm, kinetics and thermodynamics perspectives, *Environ. Nanotechnol., Monit. Manage.*, 2022, **17**, 100651.
19 S. Álvarez-Torrellas, *et al.*, Enhancement of p-nitrophenol adsorption capacity through N2-thermal-based treatment of activated carbons, *Appl. Surf. Sci.*, 2017, **414**, 424–434.
20 F. Banisheykholeslami, M. Hosseini and G. Najafpour Darzi, Design of PAMAM grafted chitosan dendrimers biosorbent for removal of anionic dyes: Adsorption isotherms, kinetics and thermodynamics studies, *Int. J. Biol. Macromol.*, 2021, **177**, 306–316.
21 E. Šehović, *et al.*, Simultaneous adsorption of heavy metals from water by novel lemon-peel based biomaterial, *Pol. J. Chem. Technol.*, 2020, **22**(1), 46–53.
22 G. Ding, *et al.*, Simultaneous adsorption of methyl red and methylene blue onto biochar and an equilibrium modeling at high concentration, *Chemosphere*, 2016, **163**, 283–289.
23 Q. Li, *et al.*, Magnetic Fe_3O_4/MnO_2 core–shell nanocomposite for removal of heavy metals from wastewater, *SN Appl. Sci.*, 2020, **2**(8), 1375.
24 T. P. Fato, *et al.*, Simultaneous Removal of Multiple Heavy Metal Ions from River Water Using Ultrafine Mesoporous Magnetite Nanoparticles, *ACS Omega*, 2019, **4**(4), 7543–7549.
25 H. Patel, Fixed-bed column adsorption study: a comprehensive review, *Appl. Water Sci.*, 2019, **9**(3), 45.
26 M. Banerjee, *et al.*, Removal of Cr(VI) from Its Aqueous Solution Using Green Adsorbent Pistachio Shell: a Fixed Bed Column Study and GA-ANN Modeling, *Water Conserv. Sci. Eng.*, 2018, **3**, 1–13.
27 K. H. Hama Aziz, *et al.*, Biochar as green adsorbents for pharmaceutical pollution in aquatic environments: A review, *Desalination*, 2024, **583**, 117725.
28 K. Hama Aziz, Removal of Toxic Heavy Metals From Aquatic Systems Using Low-cost and Sustainable Biochar: A Review, *Desalination Water Treat.*, 2024, **320**, 100757.
29 P. Zhang, *et al.*, A machine learning assisted prediction of potential biochar and its applications in anaerobic digestion for valuable chemicals and energy recovery from organic waste, *Carbon Neutrality*, 2024, **3**(1), 2.
30 J. Chang and J.-Y. Lee, Machine Learning-Based Prediction of the Adsorption Characteristics of Biochar from Waste Wood by Chemical Activation, *Materials*, 2024, **17**(21), 5359.
31 W. Zhang, *et al.*, Synthesis optimization and adsorption modeling of biochar for pollutant removal via machine learning, *Biochar*, 2023, **5**(1), 25.
32 B. Debnath, D. Haldar and M. K. Purkait, Environmental remediation by tea waste and its derivative products: A review on present status and technological advancements, *Chemosphere*, 2022, **300**, 134480.
33 S. Srivastava, R. Sinha and D. Roy, Toxicological effects of malachite green, *Aquat. Toxicol.*, 2004, **66**(3), 319–329.

34 S. I. Siddiqui, *et al.*, Investigation of Congo Red Toxicity towards Different Living Organisms: A Review, *Processes*, 2023, **11**(3), 807.
35 S. Silambarasan, P. Cornejo and A. S. Vangnai, Biodegradation of 4-nitroaniline by novel isolate Bacillus sp. strain AVPP64 in the presence of pesticides, *Environ. Pollut.*, 2022, **306**, 119453.
36 M. A. Hossain, *et al.*, Toxic effects of chlorpyrifos on the growth, hematology, and different organs histopathology of Nile tilapia, Oreochromis niloticus, *Saudi J. Biol. Sci.*, 2022, **29**(7), 103316.
37 T. Mahmood, *et al.*, Comparison of Different Methods for the Point of Zero Charge Determination of NiO, *Ind. Eng. Chem. Res.*, 2011, **50**(17), 10017–10023.
38 D. Patel, *et al.*, Surface roughness prediction of machined components using gray level co-occurrence matrix and Bagging Tree, *FME Trans.*, 2020, **48**(2), 468–475.
39 M. Shah, *et al.*, Utilizing TGAN and ConSinGAN for Improved Tool Wear Prediction: A Comparative Study with ED-LSTM, GRU, and CNN Models, *Electronics*, 2024, **13**(17), 3484.
40 I. D. Mienye, T. G. Swart and G. Obaido, Recurrent Neural Networks: A Comprehensive Review of Architectures, Variants, and Applications, *Information*, 2024, **15**(9), 517.
41 G. Y. Tang, *et al.*, Health Functions and Related Molecular Mechanisms of Tea Components: An Update Review, *Int. J. Mol. Sci.*, 2019, **20**(24), 6196.
42 F.-D. Zhang, *et al.*, Identification of Dalbergia cochinchinensis (CITES Appendix II) from other three Dalbergia species using FT-IR and 2D correlation IR spectroscopy, *Wood Sci. Technol.*, 2016, **50**, 693–704.
43 M. A. Brza, *et al.*, Tea from the drinking to the synthesis of metal complexes and fabrication of PVA based polymer composites with controlled optical band gap, *Sci. Rep.*, 2020, **10**(1), 18108.
44 S. Fan and L. Zhang, Production and characterization of tea waste–based biochar and its application in treatment of Cd-containing wastewater, *Biomass Convers. Biorefin.*, 2021, **11**(5), 1719–1732.
45 M. S. Reza, *et al.*, Biochar characterization of invasive Pennisetum purpureum grass: effect of pyrolysis temperature, *Biochar*, 2020, **2**(2), 239–251.
46 X. Li, *et al.*, Functional Groups Determine Biochar Properties (pH and EC) as Studied by Two-Dimensional (13)C NMR Correlation Spectroscopy, *PLoS One*, 2013, **8**(6), e65949.
47 K. Yang, *et al.*, Correlations and adsorption mechanisms of aromatic compounds on a high heat temperature treated bamboo biochar, *Environ. Pollut.*, 2016, **210**, 57–64.
48 X.-F. Tan, *et al.*, Role of biochar surface characteristics in the adsorption of aromatic compounds: Pore structure and functional groups, *Chin. Chem. Lett.*, 2021, **32**(10), 2939–2946.
49 A. Tomczyk, Z. Sokołowska and P. Boguta, Biochar physicochemical properties: pyrolysis temperature and feedstock kind effects, *Rev. Environ. Sci. Bio/Technol.*, 2020, **19**(1), 191–215.
50 G. Loebsack, *et al.*, Impact of biochar physical properties on adsorption mechanisms for removal of aromatic aqueous contaminants in water, *Biomass Bioenergy*, 2025, **194**, 107617.
51 M. Hou, *et al.*, Preparation of Biomass Biochar with Components of Similar Proportions and Its Methylene Blue Adsorption, *Molecules*, 2023, **28**(17), 6261.
52 M. N. N. Atirah, M. Raoov and S. Mohamad, Spent tea leaves as an adsorbent for micro-solid-phase extraction of polycyclic aromatic hydrocarbons (PAHs) from water and food samples prior to GC-FID analysis, *Microchem. J.*, 2020, **159**, 105581.
53 R. Chatterjee, *et al.*, Effect of Pyrolysis Temperature on PhysicoChemical Properties and Acoustic-Based Amination of Biochar for Efficient CO_2 Adsorption, *Front. Energy Res.*, 2020, **8**, 85.
54 M. Rafiq, *et al.*, Influence of Pyrolysis Temperature on Physico-Chemical Properties of Corn Stover (Zea mays L.) Biochar and Feasibility for Carbon Capture and Energy Balance, *PLoS One*, 2016, **11**(6), e0156894.
55 U. Kumar, *et al.*, Cleaner production of iron by using waste macadamia biomass as a carbon resource, *J. Cleaner Prod.*, 2017, **158**, 218–224.
56 D. T. M. Phuong, N. X. Loc and T. Miyanishi, Efficiency of dye adsorption by biochars produced from residues of two rice varieties, Japanese Koshihikari and Vietnamese IR50404, *Desalin. Water Treat.*, 2019, **165**, 333–351.
57 R. Chatterjee, *et al.*, Effect of Pyrolysis Temperature on PhysicoChemical Properties and Acoustic-Based Amination of Biochar for Efficient CO_2 Adsorption, *Front. Energy Res.*, 2020, **8**, 85.
58 P. Tu, *et al.*, Influence of pyrolysis temperature on the physicochemical properties of biochars obtained from herbaceous and woody plants, *Bioresour. Bioprocess.*, 2022, **9**(1), 131.
59 S. Neusatz Guilhen, *et al.*, Role of Point of Zero Charge in the Adsorption of Cationic Textile Dye on Standard Biochars from Aqueous Solutions: Selection Criteria and Performance Assessment, *Soldering Mater.*, 2022, **04**(02), 010.
60 G. Zhang, *et al.*, Highly Efficient Adsorption Characteristics and Mechanism of Nutshell Biochars for Aromatic Organophosphorus Insecticides, *Agronomy*, 2023, **13**(2), 543.
61 Q. Yu, *et al.*, Mechanisms of aromatic molecule - Oxygen-containing functional group interactions on carbonaceous material surfaces, *Chemosphere*, 2021, **275**, 130021.
62 H. J. Abdoul, *et al.*, Efficient adsorption of bulky reactive dyes from water using sustainably-derived mesoporous carbons, *Environ. Res.*, 2023, **221**, 115254.
63 S. Praveen, *et al.*, Biochar for removal of dyes in contaminated water: an overview, *Biochar*, 2022, **4**(1), 10.
64 M. Malhotra, S. Suresh and A. Garg, Tea waste derived activated carbon for the adsorption of sodium diclofenac from wastewater: adsorbent characteristics, adsorption isotherms, kinetics, and thermodynamics, *Environ. Sci. Pollut. Res.*, 2018, **25**(32), 32210–32220.
65 S. Jha, *et al.*, Kinetic and Isothermal Investigations on the Use of Low Cost Coconut Fiber-Polyaniline Composites for

the Removal of Chromium from Wastewater, *Polymers*, 2022, **14**(20), 4264.

66 J. Ederer, *et al.*, A Study of Methylene Blue Dye Interaction and Adsorption by Monolayer Graphene Oxide, *Adsorpt. Sci. Technol.*, 2022, **2022**, 7385541.

67 R. Ahmad Aftab, *et al.*, Removal of congo red from water by adsorption onto activated carbon derived from waste black cardamom peels and machine learning modeling, *Alexandria Eng. J.*, 2023, **71**, 355–369.

68 B. Kangra, *et al.*, Effective adsorption of chlorpyrifos pesticides by HKUST-1 metal-organic framework, *J. Chem. Sci.*, 2022, **134**(4), 104.

69 R. Elsharkawy, *et al.*, Adsorption study of bisphenol-A and chlorpyrifos onto nanobentonite intercalated with magnetite and sodium alginate: kinetics and isotherm models, *Int. J. Environ. Sci. Technol.*, 2022, **19**, 9827–9842.